

Tracing the large scale structure in the *Chandra* Deep Field South

R. Gilli^{1,2}, A. Cimatti¹, E. Daddi³, G. Hasinger⁴, P. Rosati³, G. Szokoly⁴, P. Tozzi⁵, J. Bergeron³, S. Borgani⁶, R. Giacconi^{2,7}, L. Kewley⁸, V. Mainieri^{3,9}, M. Mignoli¹⁰, M. Nonino⁵, C. Norman^{2,11}, J. Wang², G. Zamorani¹⁰, W. Zheng², and A. Zirm²

ABSTRACT

We report the discovery of large scale structures of X-ray sources in the 1Msec observation of the *Chandra* Deep Field South. Two main structures appear as narrow ($\Delta z \lesssim 0.02$) spikes in the source redshift distribution at $z=0.67$ and $z=0.73$, respectively. Their angular distribution spans a region at least ~ 17 arcmin wide, corresponding to a physical size of $7.3h_{70}^{-1}$ Mpc at a redshift of $z \sim 0.7$ ($\Omega_m = 0.3$, $\Omega_\Lambda = 0.7$). These spikes are populated by 19 sources each, which are mainly identified as Active Galactic Nuclei (AGN). Two sources in each spike are extended in X-rays, corresponding to galaxy groups/clusters embedded in larger structures. The X-ray source redshift distribution shows other spikes, the most remarkable at $z=1.04$, 1.62 and 2.57 . This is one of the first evidences for large scale structure traced by X-ray sources and for spatial clustering of X-ray selected AGN. The X-ray data have been complemented with the spectroscopic data from the K20 near infrared survey (Cimatti et al. 2002),

¹Istituto Nazionale di Astrofisica (INAF) - Osservatorio Astrofisico di Arcetri, Largo E. Fermi 5, 50125 Firenze, Italy

²The Johns Hopkins University, Homewood Campus, Baltimore, MD 21218

³European Southern Observatory, Karl-Schwarzschild-Strasse 2, Garching, D-85748, Germany

⁴Max-Planck-Institut für extraterrestrische Physik, Postfach 1312, D-85741 Garching, Germany

⁵Istituto Nazionale di Astrofisica (INAF) - Osservatorio Astronomico, Via G. Tiepolo 11, 34131 Trieste, Italy

⁶INFN, c/o Dip. di Astronomia dell'Università, Via G. Tiepolo 11, 34131 Trieste, Italy

⁷Associated Universities, Inc. 1400 16th Street, NW, Suite 730, Washington, DC 20036

⁸Harvard-Smithsonian Center for Astrophysics, 60 Garden Street, Cambridge, MA 02138

⁹Dip. di Fisica, Università degli Studi Roma Tre, Via della Vasca Navale 84, I-00146 Roma, Italy

¹⁰Istituto Nazionale di Astrofisica (INAF) - Osservatorio Astronomico di Bologna, Via Ranzani 1, 40127 Bologna, Italy

¹¹Space Telescope Science Institute, 3700 San Martin Drive, Baltimore, MD 21218

which covers $\sim 1/10$ of the X-ray field. Also in this survey the source redshift distribution shows several spikes. Two narrow structures at $z=0.67$ and $z=0.73$ (again with $\Delta z \sim 0.02$) are the most significant features, containing 24 and 47 galaxies, respectively. While the K20 structure at $z=0.73$ is dominated by a standard galaxy cluster with a significant concentration around a central cD galaxy and morphological segregation, the galaxies at $z=0.67$ constitute a loose structure rather uniformly distributed along the K20 field.

Moreover, we find a very good correlation (almost one-to-one) also between less prominent peaks detected in the redshift distributions of X-ray and K20 sources. In particular, at $z < 1.3$ we find that 5 out of the 6 more significant K20 peaks have a corresponding peak in the X-ray selected sources and, similarly, all the 5 X-ray peaks below that redshift have a corresponding K20 peak. Since the K20 survey sensitivity drops beyond $z \sim 1.3$, structures at higher redshift are traced only by the X-ray sources. This correlation suggests that AGN (from the X-ray data) and (early-type) galaxies (from the K20 survey) are tracing the same underlying structures.

We also compared the X-ray and K-band catalogs to search for enhanced X-ray activity in the sources in the two main redshift spikes. While in the structure at $z=0.73$ the fraction of X-ray sources is the same as in the field, in the structure at $z=0.67$ it is higher by a factor of ~ 2 , suggesting that X-ray activity may be triggered preferentially in the structure at $z=0.67$. Given the limited statistics, this result is significant only at $\sim 2\sigma$ level.

1. Introduction

While the large scale structure of the Universe at $z < 1$ is usually mapped through galaxy surveys, AGN surveys are a powerful tool to study the clustering of high redshift objects. AGN clustering has been extensively studied and detected at optical wavelengths (Shanks et al. 1987; La Franca et al. 1998; Croom et al. 2001), where objects are mainly selected by means of their strong UV excess and include almost exclusively unobscured-type 1 AGN. An advantage of the X-ray selection, especially in the hard X-rays, resides in the capability of detecting also obscured AGN, which, based on population synthesis models for the X-ray background, are believed to be a factor of 4–10 more abundant than unobscured AGN (Comastri et al. 1995; Gilli et al. 2001).

While angular clustering of X-ray selected AGN was detected by several authors (Vikhlinin & Forman 1995; Akylas et al. 2000; Giacconi et al. 2001), yet there are no direct measure-

ments of their spatial clustering. Boyle & Mo (1993) studied the AGN at $z < 0.2$ in the Einstein Medium Sensitivity Survey (EMSS, Stocke et al. 1991), without finding any positive clustering signal. Carrera et al. (1998) considered the AGN in the ROSAT International X-ray Optical Survey (RIXOS, Mason et al. 2000) and in the Deep ROSAT Survey (Boyle et al. 1994), detecting only a weak ($\sim 2\sigma$) clustering signal on scales $< 60 - 120 h_{70}^{-1}$ Mpc for the RIXOS AGN subsample in the redshift range $z = 0.5 - 1.0$.

The *Chandra* Msec surveys in the Deep Field South (CDFS, Rosati et al. 2002) and North (CDFN, Brandt et al. 2001) will allow a step forward in the detection of X-ray source structures. A large spectroscopic identification program down to very faint magnitudes ($R < 25.5$) is underway in the CDFS, which is expected to provide reliable redshift estimates for $\sim 70\%$ of the X-ray sample. Although 10 – 20% of the sources in the deep X-ray surveys are identified as normal/starburst galaxies, still AGN are the dominant population (Giacconi et al. 2001; Barger et al. 2002). In this paper we will consider the redshift distribution of those CDFS sources for which a robust redshift determination is already available ($\sim 38\%$ of the full sample). This distribution shows two prominent spikes at $z = 0.67$ and $z = 0.73$ (see also Hasinger 2002) as well as several other spikes at higher redshift. Narrow spikes are commonly detected in the redshift distribution of optical galaxies observed in deep pencil beam surveys (Le Fevre et al. 1996; Cohen et al. 1999), and are now being observed also among X-ray selected objects. Narrow structures at $z \sim 0.8$ and $z \sim 1$, similar to those observed in the CDFS, are indeed observed also in the CDFN (Barger et al. 2002).

In this paper the features in the redshift distribution of X-ray sources in the CDFS are compared with those observed in the K20 survey (Cimatti et al. 2002), which efficiently selects massive galaxies in a broad redshift range and covers part of the CDFS field. In addition, the X-ray and K20 catalogs are cross correlated to search for any enhanced X-ray activity in the two main redshift structures with respect to the field. We note that a concentration of objects at $z=0.67$ in the CDFS (mostly early type galaxies) was also reported by Croom, Warren & Glazebrook (2001), who selected objects with $K \leq 19.5$ and $J - K$ colors redder than the stellar sequence.

The analysis of the spatial clustering of the full X-ray sample and the comparison with the spatial clustering of K20 sources will be presented in a future paper.

Throughout this paper we will use a cosmology with $H_0 = 70 \text{ km s}^{-1} \text{ Mpc}^{-1}$, $\Omega_m = 0.3$, $\Omega_\Lambda = 0.7$.

2. X-ray sources

The CDFS has been observed for 1Msec with ACIS-I, and represents one of the deepest X-ray surveys to date (Rosati et al. 2002). Limiting fluxes of $5.5 \cdot 10^{-17}$ erg cm $^{-2}$ s $^{-1}$ and $4.5 \cdot 10^{-16}$ erg cm $^{-2}$ s $^{-1}$ have been reached in the 0.5-2 keV and 2-10 keV band, respectively; 346 sources have been detected in the whole 0.1 deg 2 field. The full X-ray catalog and the details of the detection process have been presented by Giacconi et al. (2002). The optical follow-up was primarily performed using the FORS1 camera at the VLT. The combined R band data cover a 13.6×13.6 arcmin field to limiting magnitudes between 26 and 26.7. In the CDFS area not covered by FORS mosaics, we used shallower data from the ESO Imaging Survey (EIS, Arnouts et al. 2001). The optical identification process is described in Tozzi et al. (2001) and Giacconi et al. (2001). Optical spectroscopy for most of the X-ray counterparts with $R < 25.5$ has been obtained with FORS1 during several observational runs at VLT. The analysis of the spectroscopic data is almost completed. The details of the data reduction, as well as the final redshift list, will be presented in Szokoly et al. (in preparation). So far 169 redshifts have been obtained. Quality flags have been assigned to the spectra, according to their reliability. Here we consider only the 121 sources with a quality flag $Q = 2$ (excluding a few stars), where two or more emission lines have been observed and the redshift determination is unambiguous, plus 10 sources whose redshift is determined from the cross-correlation with K20 sources. The sample includes sources detected either in the soft (0.5-2 keV) or in the hard (2-10 keV) band or both. The 1σ errors on the redshift measurements are typically of the order of $\Delta z \sim 0.002$. The redshift distribution is dominated by two large concentrations of sources in the ranges $0.664 \leq z \leq 0.685$ and $0.725 \leq z \leq 0.742$ containing 19 objects each. In the following we will refer to these two structures as *sources at $z = 0.67$* and *sources at $z = 0.73$* , respectively. These striking structures can be seen in the upper panel of Figure 1, where we plot the redshift distribution of X-ray sources in redshift bins of $\Delta z = 0.02$. Due to the fixed bin width, both structures appear to contain 18 rather than 19 sources. Other possible, less prominent structures (see Section 4) are clearly visible in this plot.

As shown in Figure 2, sources at $z=0.67$ and $z=0.73$ are mostly distributed in one half of the field. Since the spectroscopic coverage of the CDFS is rather uniform (Szokoly et al., in preparation), the higher concentration of sources in half of the field is not likely to be an artifact. The structures extend to a scale of ~ 17 arcmin, corresponding to a linear physical size of 7.3 Mpc at $z \sim 0.7$. This is likely to be a lower limit, since the source angular distribution appears to be limited only by the finite size of the X-ray image. Two extended sources (CDFS 560, 645), identified as two galaxy groups, are present in the structure at $z=0.67$. Similarly, two extended sources (CDFS 594, 566) belong to the structure at $z=0.73$: one is identified as a galaxy group, the other is associated with the galaxy cluster in the

K20 survey (see next Section and Fig. 2 and 3). The full list of CDFS extended sources is given in Giacconi et al. (2002). Preliminary results on the CDFS extended sources are being obtained from XMM observations: while CDFS 566 is not sufficiently extended to be resolved by XMM, CDFS 594 appears to be a factor of ~ 4 more extended than measured by *Chandra* (J. Bergeron, priv. comm.).

In addition to the above discussed structures, smaller peaks are also recognized in the X-ray source redshift distribution. To assess the significance of these structures we follow a procedure similar to that adopted by Cohen et al. (1999), who observed features in their galaxy redshift distribution with typical velocity dispersion of ~ 300 km/s. Sources are distributed in $V = c \ln(1 + z)$ rather than in redshift, since dV corresponds to local velocity variations granted the Hubble expansion. The observed distribution is then smoothed with a Gaussian with $\sigma_S = 300$ km/s to obtain the “signal” distribution. Since there is no a priori knowledge of the “background” field distribution, we heavily smoothed the observed distribution with a Gaussian with $\sigma_B = 1.5 \cdot 10^4$ km/s and considered this as the background distribution.

We then searched for possible redshift peaks in the signal distribution, computing for each of them a signal-to-noise ratio defined as $SNR = (S - B) / \sqrt{B}$, where S is the number of sources in a velocity interval of fixed width $\Delta V = 2000$ km/s around the center of each peak candidate and B is the number of background sources in the same interval. The value of ΔV was chosen to optimize the SNR values for peaks populated by 3-5 sources. For more populated peaks the quantity S may underestimate the actual number of sources in each peak. Adopting the thresholds $S \geq 3$ and $SNR > 3.8$ we find 7 peaks in the signal distribution. In order to estimate the expected fraction of possibly “spurious” peaks arising from background fluctuations, we simulated 1000 samples of 131 redshifts randomly extracted from the smoothed background distribution and applied our peak detection method to each simulated sample. The result is that, with the adopted thresholds, the average number of spurious peaks due to background fluctuations is 0.47. In only 13 of the simulated samples 3 spurious peaks are detected, while in none of simulated samples 4 or more spurious peaks are detected.

The seven X-ray source peaks detected by our procedure with $S \geq 3$ and $SNR > 3.8$ are listed in Table 1, where for each peak we give the average redshift, the number of objects (N) in the peak and the Poissonian probability of observing N sources given the background value in the same velocity intervals where the N sources are found.

We checked our detection method with larger values of the smoothing length for the signal distribution. We verified that, when increasing σ_S , several peaks are lost; as an example, when the signal smoothing is as large as 1500 km/s, corresponding to the velocity

dispersion of rich clusters, only the three most significant peaks at $z=0.67$, 0.73 and 1.62 are detected. Therefore we will consider only the results obtained with $\sigma_S = 300$ km/s in the following.

3. Sources from the K20 survey

Part of the CDFS field has been covered by the K20 survey (see Cimatti et al. 2002 and references therein), which includes all the sources detected in the EIS K-band images to $K_s < 20$. The K20 field (6.7 by 4.8 arcmin) covers $\sim 1/10$ of the X-ray field, and is shown as a rectangle in Figure 2: 348 sources with $K_s < 20$ have been found in this area. Spectroscopic identification of the K20 sources has been performed with FORS1 and FORS2 at the VLT. We will consider here only the 258 galaxies with highest quality spectra and unambiguous redshift determination. The typical error on the redshift estimate is $\Delta z = 0.002$. The redshift distribution of the K20 sources in bins of $\Delta z = 0.02$ is shown in the lower panel of Figure 1. In strict analogy with the X-ray results, the redshift distribution of the K20 galaxies has two prominent peaks at $z=0.67$ and $z=0.73$.

While in the X-rays the two structures at $z=0.67$ and $z=0.73$ appear equally populated, in the smaller K20 field sources at 0.73 (47 objects) are a factor of ~ 2 more numerous than sources at 0.67 (24 objects). The redshift ranges defining the two spikes are the same adopted for X-ray sources ($0.664 \leq z \leq 0.685$ and $0.725 \leq z \leq 0.742$). Again, due to the fixed bin size adopted in Fig. 1, only 45 and 22 sources appear in the spikes at $z=0.73$ and $z=0.67$, respectively.

Inspection of the distribution on the sky of the K20 sources together with their spectral properties reveals that the two structures are indeed very different. The structure at $z = 0.73$ appears to be dominated by a standard galaxy cluster, showing a central cD galaxy and significant spectral segregation, with early type objects concentrated around the cD galaxy. Overall, 25 out of 47 sources at $z = 0.73$ are classified as early type galaxies, 17 are emission line galaxies, 4 have intermediate spectra, and 1 object has been recognized as an AGN. Sixteen out of 19 K20 sources within a circle of radius 1 arcmin (~ 440 Kpc) around the central cD are early type objects (see Fig. 3). On the contrary, sources at $z = 0.67$ constitute a loose structure with early and late type galaxies uniformly distributed across the K20 field. For completeness, we note that 11 out of 24 sources at $z = 0.67$ are classified as early type galaxies, 11 are late type galaxies and 2 have intermediate spectra.

We have searched for other peaks in the K20 redshift distribution using the same procedure described in the previous Section. Adopting the same parameters as in the analysis

of the X-ray data for the smoothing lengths ($\sigma_S = 300$ km/s and $\sigma_B = 1.5 \cdot 10^4$ km/s) and similar values for the thresholds in SNR and S ($SNR > 4.0$ and $S \geq 4$) we find 8 peaks. Also in this case the average number of spurious peaks, obtained from 1000 simulated samples, is low (0.11). None of the simulated samples contains 3 or more spurious peaks. The central redshifts, number of sources, and Poissonian probability related to the K20 peaks are quoted in Table 1.

Inspection of Table 1 reveals that, besides the two prominent spikes at $z=0.67$ and $z=0.73$, other peaks are in common between the K20 and the X-ray data. The third most populated K20 peak (15 sources at $z=1.036$) is detected also in the X-rays, being the third populated peak of the X-ray redshift distribution (6 sources). Another two K20 peaks (at $z \sim 0.077$ and 1.220) have a corresponding peak in the X-ray source redshift distribution. Overall, 5 out of 8 peaks in the K20 source redshift distribution have an X-ray peak counterpart. If we restrict our analysis to the more significant K20 peaks with Poissonian probability smaller than 10^{-3} and $5 \cdot 10^{-4}$, the fraction with X-ray counterpart is $5/6$ and $4/4$, respectively. The fact that the less significant K20 peaks do not have a corresponding X-ray peak may be expected since the total number of X-ray sources is much lower (a factor of ~ 2) than that of K20 sources and is spread over a wider redshift range. Only about 30% of the X-ray sources in these peaks is within the area covered by the smaller K20 survey. This means that, in general, the structures seen in the K20 survey are traced on wider scales by the X-ray sources. We note that the high redshift peaks detected in the X-rays are not detected in the K20 observations, whose sensitivity drops dramatically above $z \sim 1.3$.

4. The X-ray source fraction in the redshift structures

4.1. Total X-ray sample

Since enhanced nuclear or star forming activity (both marked by X-ray emission) are likely to be produced by galaxy interactions in large scale structures, we searched for any variation in the X-ray to K20 source number ratio inside and outside the two structures at $z=0.67$ and $z=0.73$.

First, we simply divided the number of X-ray sources by the number of K20 sources inside and outside the two structures to search for variations with respect to the field. Extended X-ray sources (two in each structure) have been excluded from this analysis. Despite the significant spectroscopic incompleteness in the X-ray sample ($\sim 60\%$ of the CDFS sources have no secure redshift determination yet), the results of this analysis should not be biased as long as the X-ray spectroscopic incompleteness is “random” with respect to the probability

of an X-ray source being inside or outside an overdensity. Since the redshift distributions of the two samples are different, in estimating the number of sources in the “field” we considered only the sources not belonging to the two structures in a redshift range centered at the redshift of the two structures. Unfortunately, given the limited statistics, this range can not be too small. Adopting the redshift range 0.4–1.0, we find that the X-ray to K-band number ratio is 0.33 ± 0.07 in the field (this ratio would be similar, but with a larger uncertainty, if we adopted the narrower redshift range 0.5–0.9), 0.36 ± 0.10 in the higher redshift spike and 0.71 ± 0.22 in the lower redshift spike. Given the relatively large errors, these ratios are all consistent with each other, even if the higher value in the lower redshift spike suggests that X-ray activity may be enhanced in this structure.

We note that most of the X-ray sources are identified as AGN on the basis of their optical and X-ray properties. Whenever the optical classification is uncertain, we considered as AGN those sources satisfying at least one the following conditions: $L_x > 10^{42}$ erg s⁻¹, where L_x is the observed luminosity in the 0.5-10 keV band; $HR > 0$, where HR is the X-ray hardness ratio; $f_x/f_r > 0.1$, where f_x and f_r are the fluxes in the 0.5-10 keV and R band, respectively. Indeed, normal and starburst galaxies typically do not exceed luminosities of 10^{42} erg s⁻¹ (e.g. Fabbiano et al. 1992) and have X-ray to optical flux ratios an order of magnitude smaller than those of AGN (Stocke et al. 1991). Also, starburst spectra cannot be as hard as those of heavily obscured AGN: we verified that an average starburst template derived from Dahlem et al. (1998) would always produce $HR < 0$ in our observations. Overall, 101 out of the 131 X-ray sources in our sample are classified as AGN. Fifteen AGN are found in the $z = 0.67$ spike and 16 in the $z = 0.73$ spike, to be compared with the total number of 17 X-ray point-like sources in each spike. As a consequence, the results of the above analysis would be essentially the same if only sources identified as AGN were considered.

4.2. X-ray to K20 matched sample

The results presented in the previous Section are based on the comparison of data from two surveys (X-ray and K20) which cover different areas. In order to further check the possible significance of the enhanced X-ray activity among the sources at $z=0.67$, we have studied in more detail the correlation between the K20 sources and the 49 X-ray sources detected within the K20 field.

First we searched for any K20 counterpart of an X-ray source within a radius of 10 arcsec, choosing as the most likely counterpart candidate the K20 source closer to the X-ray source. Then we computed the RA and DEC offset histograms and fitted them with a Gaussian. The Gaussian width resulted to be $\epsilon_{RA} = 0.55$ arcsec and $\epsilon_{DEC} = 0.50$ arcsec for

the RA and DEC histogram respectively. We then corrected the K-band coordinates for the systematic shift with respect to the X-ray coordinates and searched for the K20 counterpart in a circle with radius = 1.77 arcsec (3.4ϵ , where ϵ is the average between ϵ_{RA} and ϵ_{DEC}) around the X-ray source position. We recall that, given a circular Gaussian of width ϵ , a circle of radius 3.4ϵ encloses 99.7% of the volume and then corresponds to the 3σ error box.

The cross correlation produced 30 matches between X-ray and K-band sources (then 19 X-ray sources in the K20 field have no counterpart down to $K_s < 20$). Given the surface density of K20 and X-ray sources, we estimate that the expected number of spurious chance coincidences among these X-ray and K20 matches is of the order of one.

We note that the positional match has been done using the coordinates of the X-ray source centroids rather than those of the optical counterparts, which are typically separated by $\sim 0.5 \text{ arcsec}$ from the X-ray centroids. Using the coordinates of the optical counterparts rather than those of the X-ray sources would not affect our results.

Although our adopted match radius might not be appropriate in the case of extended X-ray sources, we note that only two X-ray sources falling in the K20 field are extended. Both of them have K20 counterparts and are examined separately. With our adopted search radius, a unique K20 counterpart is found for the extended source CDFS 566, which coincides with the cD galaxy at the center of the cluster at $z = 0.73$. The other extended source, CDFS 511, can be associated to any of three K20 sources with redshifts between 0.765 and 1.047, and its identification remains uncertain. For all the 28 point-like X-ray sources with a K20 counterpart, this is unique. Only three out of 30 matches do not have a high quality redshift determination either from the K-band or the X-ray catalog. We verified that for the 20 sources with high quality redshifts both in the X-ray and in the K20 catalog the two measurements are always in excellent agreement, with essentially zero offset and a dispersion of $\Delta z = 0.003$. It is interesting to note that a large fraction (8/18) of the sources classified as AGN in the X-ray catalog were not recognized as such in the K20 spectroscopic data alone.

We then estimated the fraction of K-band selected sources detected in the X-rays inside and outside the two structures, excluding extended X-ray sources. Again an excess of X-ray sources in the low redshift spike appears. The fraction of X-ray detected sources in the low redshift spike is 0.21 ± 0.10 (5/24), while it is 0.08 ± 0.04 both in the high redshift spike (4/47) and in the neighboring redshift bins (i.e. in the range $0.4 < z < 1.0$).

Since we are now dealing with a sample free from selection biases, we tried to estimate the significance of the X-ray source overdensity at $z = 0.67$. Since 25 X-ray to K20 matches are point-like sources with measured redshift, we simulated 10000 samples of 25 sources randomly extracted from the K20 spectroscopic catalog, finding that in only 5.7% of the

cases these random samples contain 5 or more sources at $z=0.67$ (i.e. in the redshift interval 0.664–0.685). We can therefore conclude that the X-ray source enhancement in the low redshift spike is statistically significant at about 2σ level. A similar level of significance is found by restricting this analysis to the 18 matches identified with AGN (4 of which are at $z=0.67$).

5. Discussion

Our results show that in the CDFS several large scale structures of X-ray sources (mostly AGN) are being detected, which appear as narrow spikes in the source redshift distribution. The most prominent structures are detected at $z=0.67$ and $z=0.73$, while other peaks appear at higher redshifts.¹² In the CDFN Barger et al. (2002) found evidence for similar redshift spikes at $z=0.843$ and 1.017 with at least ten X-ray sources each. Despite several efforts in the past years, before the deep X-ray surveys by *Chandra* there was no convincing evidence for three-dimensional clustering of X-ray selected AGN. Only a 2σ detection was found by Carrera et al. (1998) in the ROSAT International X-ray Optical Survey (RIXOS, Mason et al. 2000) on scales $< 60 - 120 h_{70}^{-1}$ Mpc. Interestingly, the 2σ signal detected in the RIXOS refers to the subsample of sources in the redshift range 0.5–1.0, where the biggest structures in the *Chandra* deep fields are also detected, although the lack of clustering signal at $z < 0.5$ and $z > 1$ might be due to the small volume sampled and to the falling sensitivity of the RIXOS, respectively.

Significant clustering signal of X-ray selected AGN was found from two dimensional analysis based on the angular correlation function (e.g. Akylas et al. 2000; Vikhlinin & Forman 1995). The clustering length of local X-ray selected AGN was found to be similar to that of local galaxies, supporting the idea that active nuclei are unbiased with respect to normal galaxies. This was also reported by Smith et al. (1995) who found that the amplitude of the low-redshift ($z < 0.3$) QSO-galaxy angular cross-correlation function is identical to that of the APM galaxy angular correlation function, implying that QSO inhabit environments similar to those of normal galaxies. Brown, Boyle & Webster (2001) showed that in the redshift range $0.2 < z < 0.7$ the spatial cross-correlation of AGN with early type galaxies is much stronger than that between AGN and late type galaxies. We found that 80% of the highly significant peaks seen in the K20 source redshift distribution, in the range

¹²We note in passing that even removing the two structures at $z=0.67$ and $z=0.73$, the X-ray source redshift distribution in the CDFS shows an excess at $z < 1$ with respect to the predictions of standard synthesis models of the X-ray background (Comastri et al. 1995; Gilli et al. 2001).

$0.5 < z < 1.3$, have a corresponding peak in the X-rays. This supports the idea that at these redshifts AGN and early type galaxies, whose detection rate is higher in K-band than in optically selected samples, are tracing the same underlying structures.

Since the large scale structures at $z = 0.67$ and $z = 0.73$ appear as narrow spikes in the source redshift distribution and span the whole *Chandra* field of view, we verified whether they can be actually considered as “sheets”, i.e. nearly bi-dimensional structures, or filaments of galaxies as predicted by cosmological models of structure formation. The structures at $z = 0.67$ and $z = 0.73$ have an observed thickness of 18.8 Mpc and 13.4 Mpc respectively (the redshift range covered by sources at $z = 0.67$ is slightly larger than that covered by sources at $z = 0.73$), to be compared with their 7.3 Mpc extension on the plane of the sky. Given the errors on the redshift measurements, the values obtained for the physical thickness of the structures are likely to be upper limits. Furthermore, if these structures do not lay exactly on the plane of the sky, any projection effects would broaden their apparent thickness. We verified that for the broader structure at $z = 0.67$ sources at higher right ascension tend to have smaller redshifts. This projection effect needs however better statistics to be quantified. We finally note that 7.3 Mpc is likely to be a lower limit to the angular extension of the two structures, which cover almost entirely the *Chandra* field of view. Given the above uncertainties, an enlarged field and increased source statistics are needed to determine the geometry of the two structures.

We searched for enhanced X-ray activity at $z = 0.67$ and $z = 0.73$ by cross-correlating the X-ray and the K20 catalogs and looking at the fraction of K20 sources with X-ray counterparts at different redshifts. Five out of 47 K20 sources at $z = 0.73$ match an X-ray source: one is the extended source CDFS 566 and is associated to the cD galaxy of the rich cluster seen in the K20 survey; one is classified as a normal galaxy and the remaining three sources are identified as AGN. Five out of 24 K20 sources at $z = 0.67$ do show X-ray emission: one is classified as a normal galaxy, while the remaining four are classified as AGN. We found a weak (2σ) X-ray source overdensity in the structure at 0.67 with respect to the field and to the other structure at $z = 0.73$. This overdensity is also observed with the same significance when considering only those X-ray sources identified as AGN. While in the X-rays the two structures are very similar (same number of sources, similar angular extent and redshift thickness), in the K20 survey they appear very different. The K20 sources at $z = 0.73$ are dominated by a virialized galaxy cluster, with a central cD galaxy and spectral segregation, with early type galaxies clustered in the inner regions. On the contrary the K20 sources at $z = 0.67$ do not appear to constitute a galaxy cluster, being uniformly distributed across the K20 field. We note incidentally that $> 50\%$ of the K20 sources classified as early type galaxies lay in the two structures at $z = 0.67$ and $z = 0.73$ and that a concentration of early type galaxies at 0.67 in the CDFS was also reported by Croom, Warren & Glazebrook

(2001). The difference between the two structures when observed by the K20 survey can be ascribed to the small region covered by the K20 survey, which has sampled a rich cluster at $z=0.73$ without sampling any cluster at $z = 0.67$. Since the two structures are very similar in the X-rays, we might speculate that, in a region free from clusters, we would have observed an X-ray source overdensity even at $z = 0.73$. In principle, this suggests that X-ray activity in the large scale structures is triggered preferentially away from the higher density peaks corresponding to galaxy clusters. However, further work is necessary to increase the source statistics and test this idea.

6. Conclusions and future work

Our main results can be summarized as follows:

- 1) Several large scale structures of X-ray sources (mostly AGN) are being detected in the *Chandra* Deep Field South, which appear as narrow spikes in the source redshift distribution. The most prominent structures are detected at $z=0.67$ and $z=0.73$. In addition, high redshift structures are significantly detected at $z=1.04$, 1.62 and 2.57 . This represents one of the first evidences for spatial clustering of X-ray selected AGN.
- 2) Similar redshift structures, the most prominent at $z = 0.67$ and $z = 0.73$, are observed among the K-band selected galaxies of the K20 survey. About 80% of the most significant peaks in the redshift distribution of K20 sources have a corresponding peak in the X-rays. Since only a fraction of the X-ray sources in these peaks is within the smaller K20 field, we can conclude that, in general, the structures seen in the K20 survey are traced on wider scales by the X-ray sources. We also notice that, since the K20 survey sensitivity drops above $z \sim 1.3$, high redshift structures are detected only in the X-rays.
- 3) By cross-correlating the K20 and the X-ray catalog we find a weak evidence ($\sim 2\sigma$) of enhanced nuclear activity among the K20 sources at $z = 0.67$ with respect to the field, suggesting a preferential trigger in this structure. Given its low significance, this result has to be confirmed by further observations.

Significant improvements in the understanding of the large scale structures in the CDFS is expected from the on going and planned multiwavelength observations of the field. The XMM deep pointing (500 ksec in a 30 arcmin diameter region; Hasinger et al. 2002) is actually expanding the area covered by X-ray data by a factor of ~ 2 . Accurate photometric redshifts for the optically faint X-ray sources are being obtained from FORS optical images and ISAAC near-IR data and will be refined further using data from the Advanced Camera for Survey (ACS) on HST.

We wish to thank the referee for useful comments.

REFERENCES

- Akylas, A., Georgantopoulos, I., Plionis, M. 2000, MNRAS, 318, 1036
- Arnouts, S., Vandame, B., Benoist, C., et al. 2001, A&A, 379, 740
- Boyle, B.J., & Mo, H.J. 1993, MNRAS, 260, 925
- Boyle, B. J., Shanks, T., Georgantopoulos, I., Stewart, G. C., Griffiths, R. E. 1994, MNRAS, 271, 639
- Barger, A.J., Cowie, L.L., Brandt, W.N., Capak, P., Garmire, G.P., Hornschemeier, A.E., Steffen, A.T., Wehner, E.H. 2002, AJ, in press [astro-ph/0206370]
- Brandt, W.N., Alexander, D.M., Hornschemeier, A.E., et al. 2001, AJ, 122, 2810
- Brown, M.J.I., Boyle, B.J. & Webster, R.L. 2001, AJ, 122, 26
- Carrera F.J., Barcons, X., Fabian, A.C., Hasinger, G., Mason, K.O., McMahon, R.G., Mittaz, J.P.D., Page, M.J. 1998, MNRAS, 299
- Cimatti, A., Mignoli, M., Daddi, E., et al. 2002, A&A, 392, 395
- Cohen, J.G., Blandford, R., Hogg, D.W., Pahre, M.A., Shopbell, P.L. 1999, ApJ, 512, 30
- Comastri, A., Setti, G., Zamorani, G., Hasinger, G. 1995, A&A, 296, 1
- Croom, S.M., Warren, S.J., Glazebrook, K. 2001, MNRAS, 328, 150
- Croom, S.M., Shanks, T., Boyle, B.J., Smith, R.J., Miller, L., Loaring, N.S., Hoyle, F. 2001, MNRAS, 325, 483
- Dahlem, M., Weaver, K., & Heckman, T. 1998, ApJS, 118, 40
- Fabbiano, G., Kim, D.-W., & Trinchieri, G. 1992, ApJS, 80, 531
- Giacconi, R., Rosati, P., Tozzi, P., Nonino, M., Hasinger, G., Norman, C., Bergeron, J., Borgani, S., Gilli, R., Gilmozzi, R. & Zheng, W. 2001, ApJ, 551, 624
- Giacconi, R., Zirm, A., Wang, J., Rosati, P., Nonino, M., Tozzi, P., Gilli, R., Mainieri, V., Hasinger, G., Kewley, L., Bergeron, J., Borgani, S., Gilmozzi, R., Grogin, N., Koekemoer, A., Schreier, E., Zheng, W., Norman, C. 2002, ApJS, 139, 369

- Gilli, R., Salvati, M., & Hasinger, G. 2001, *A&A*, 366, 407
- Hasinger, G., et al. 2002, *ESO Msngr*, 108, 11
- La Franca, F., Andreani, P., & Cristiani, S., 1998, *ApJ*, 497, 529
- Le Fevre, O., Hudon, D., Lilly, S. J., Crampton, David, Hammer, F., Tresse, L. 1996, *ApJ*, 461, 534
- Mason, K. O., Carrera, F. J., Hasinger, G., et al. 2000, *MNRAS*, 311, 456
- Hornschemeier, A., et al. 2000, *ApJ*, 541, 49
- Shanks, T., Fong, R., Boyle, B.J., Peterson, B.A. 1987, *MNRAS*, 277, 739
- Smith, R.J., Boyle, B.J., Maddox, S.J. 1995, *MNRAS*, 277, 270
- Smith, R.J., Boyle, B.J., Maddox, S.J. 2000, *MNRAS*, 313, 252
- Stocke, John T., Morris, Simon L., Gioia, I. M., Maccacaro, T., Schild, R., Wolter, A., Fleming, Thomas A., Henry, J. P. 1991, *ApJS*, 76, 813
- Rosati, P., Tozzi, P., Giacconi, R., Gilli, R., Hasinger, G., Kewley, L., Mainieri, V., Nonino, M., Norman, C., Szokoly, G., Wang, J. X., Zirm, A., Bergeron, J., Borgani, S., Gilmozzi, R., Grogin, N., Koekemoer, A., Schreier, E., Zheng, W. 2002, *ApJ*, 566, 667
- Tozzi, P., Rosati, P., Nonino, M., Bergeron, J., Borgani, S., Gilli, R., Gilmozzi, G., Hasinger, G., Grogin, N., Kellerman, K., Kewley, L., Koekemoer, A., Norman, C., Schreier, E., Shaver, P., Wang, J.X., Zheng, W., Zirm, A. & Giacconi, R. 2001, *ApJ*, 562, 42
- Vikhlinin, A., Forman, W. 1995, *ApJ*, 455, L109

z	K20		X-ray	
	N	Prob.	N	Prob.
0.077	5	$4.9 \cdot 10^{-4}$	3	$1.0 \cdot 10^{-2}$
0.218	5	$3.3 \cdot 10^{-2}$		
0.367	7	$3.7 \cdot 10^{-2}$		
0.524	11	$6.0 \cdot 10^{-4}$		
0.670	24	$1.9 \cdot 10^{-4}$	19	$9.1 \cdot 10^{-5}$
0.738	47	$6.0 \cdot 10^{-8}$	19	$1.7 \cdot 10^{-6}$
1.036	15	$6.4 \cdot 10^{-4}$	6	$4.2 \cdot 10^{-3}$
1.220	10	$3.2 \cdot 10^{-4}$	4	$2.2 \cdot 10^{-2}$
1.618			5	$3.8 \cdot 10^{-3}$
2.572			4	$9.7 \cdot 10^{-3}$

Table 1: Peaks detected in the X-ray and K20 source redshift distributions, sorted by increasing redshift. The signal and background distributions are smoothed with $\sigma_S = 300$ km/s and $\sigma_B = 1.5 \cdot 10^4$ km/s, respectively. Together with the central redshift of each peak, the number of sources N in each peak and the Poissonian probability of observing N or more sources given the background value are also shown.

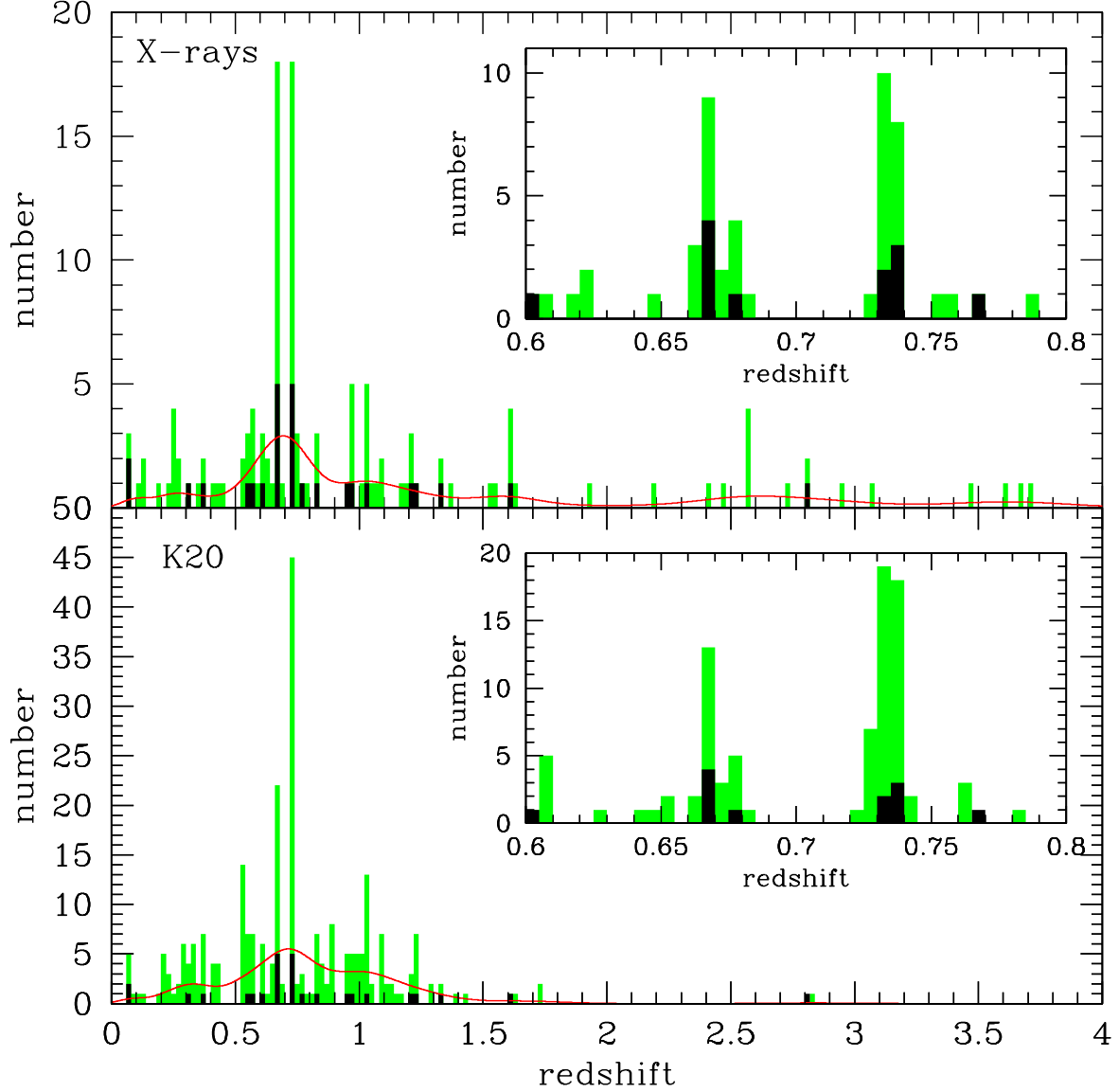


Fig. 1.— Redshift distribution for X-ray sources (Upper Panel) and K20 sources (Lower Panel) with high quality optical spectra. The binning shown in this Figure is $\Delta z = 0.02$. The insets show a zoom on the two main redshift spikes at $z=0.67$ and $z=0.73$ (binning is $\Delta z = 0.005$). The black histograms represent the matches between the X-ray and the K20 catalogs. The “background” field distributions, derived by smoothing the observed ones with $\sigma_B = 1.5 \cdot 10^4$ km/s (see text), are shown as continuous lines.

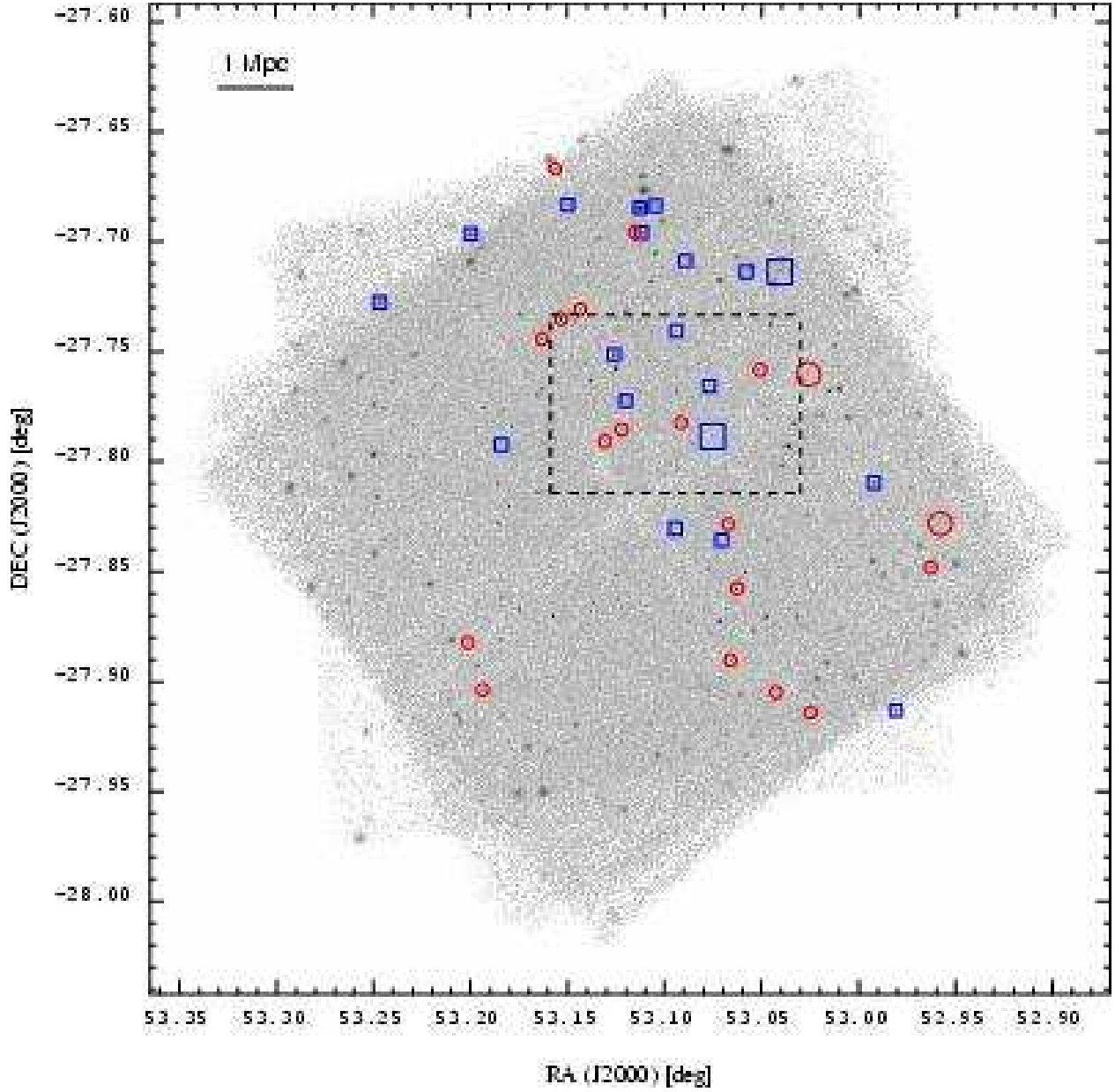


Fig. 2.— *Chandra* ACIS-I image of the CDFS with the sources in the two redshift spikes marked with different symbols: circles for sources at $z = 0.67$ and squares for sources at $z = 0.73$. Extended sources in the spikes are represented as big symbols. The ACIS-I detector is ~ 17 arcmin on a side. The dashed box indicates the 6.7×4.8 arcmin region covered by the K20 survey.

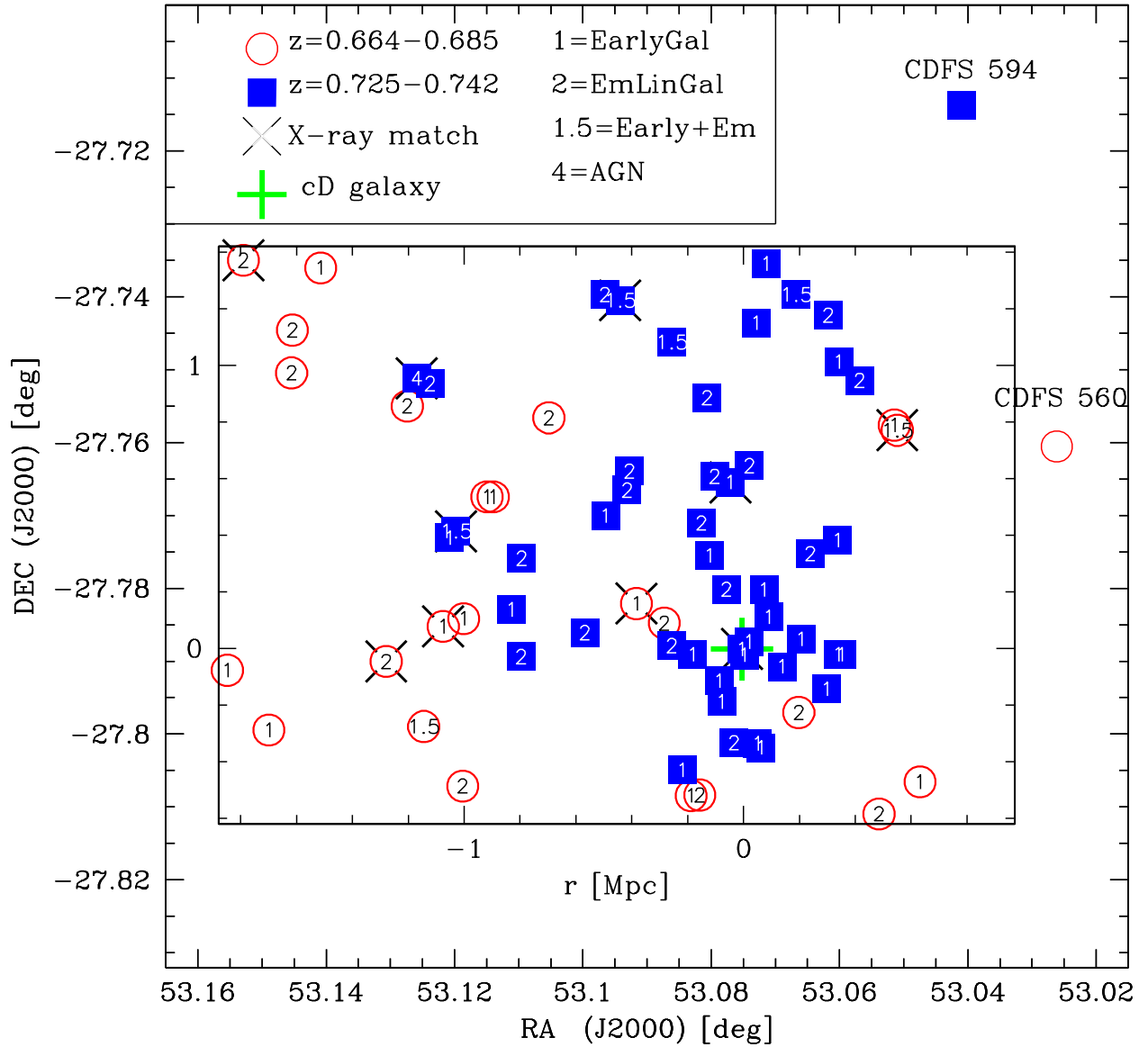


Fig. 3.— Spatial distribution of the K20 sources at $z = 0.67$ (open circles) and at $z = 0.73$ (filled squares). Their classification from K20 spectroscopy is also indicated by the numbers inside the symbols. Crosses are overplotted on sources with X-ray counterparts. Sources at $z = 0.73$ appear to constitute a standard galaxy cluster with a cD galaxy marking its center (indicated by the big cross) and showing spectral segregation, with early type galaxies concentrated in the inner regions. On the contrary, sources at $z = 0.67$ do not cluster around any cD galaxy and are uniformly distributed across the field. One galaxy group at $z=0.67$ (CDFS 560) and one at $z=0.73$ (CDFS 594) detected in the X-rays just outside the K20 field are also indicated.